Coupled Assimilation of Geostationary Satellite Sounder Data into a Mesoscale Model Using the Bratseth Analysis Approach

FRANK H. RUGGIERO

Battlespace Environment Division, Air Force Research Laboratory, Hanscom AFB, Massachusetts

KEITH D. SASHEGYI

Remote Sensing Division, Naval Research Laboratory, Washington, D.C.

ALAN E. LIPTON*

Battlespace Environment Division, Air Force Research Laboratory, Hanscom AFB, Massachusetts

RANGARAO V. MADALA

Remote Sensing Division, Naval Research Laboratory, Washington, D.C.

SETHU RAMAN

Department of Marine, Earth, and Atmospheric Sciences, North Carolina State University, Raleigh, North Carolina

(Manuscript received 6 February 1997, in final form 26 May 1998)

ABSTRACT

A satellite–model coupled procedure for assimilating geostationary satellite sounder data was adapted to a mesoscale analysis and forecast system jointly developed by the Naval Research Laboratory and the Air Force Research Laboratory. The coupled procedure involves the use of the model output fields as the first guess for the thermodynamic retrievals. Atmospheric thermodynamic profiles and ground temperatures were retrieved from observed radiances of the VISSR Atmospheric Sounder (VAS) on board the Geostationary Operational Environmental Satellite. The successive corrections objective analysis scheme in the mesoscale analysis and forecast system was modified to consider the horizontal spatial correlation of the satellite data. The procedure was tested using a wintertime case from the 1986 Genesis of Atlantic Lows Experiment project. The retrievals generated by the coupled method were modestly improved relative to independent stand-alone retrievals. Coupled analyses and forecasts of temperature and moisture fields compared favorably to forecasts from a control run without the VAS assimilation.

1. Introduction

As the focus shifts in operational weather forecasting to use of mesoscale models with increasingly high resolution, the need exists to introduce data of sufficient resolution to provide for the initial fields. Atmospheric remote sounders, on board the Geostationary Operational Environmental Satellites (GOES) since 1980, are a readily available source of mesoscale information. Indeed, their high horizontal and temporal resolutions are ideally suited to mesoscale analyses and forecast models. However, the parameters observed by the GOES sounders are not model prognostic variables but are measures of spectral radiation, which can be represented as infrared brightness temperatures. These brightness temperatures are taken at various wavelengths associated with emissions from the earth's surface and atmospheric gases. The information from the sounder may be converted to meteorologically useful information using radiative transfer theory. Converting the brightness temperatures to ground and atmospheric temperatures and moisture is complicated by the fact that the solution to the problem is not unique. The nonuniqueness is inherent in the integral nature of radiative transfer in the atmosphere and is a significant problem because the integration is over a broad enough depth of the atmo-

* Current affiliation: Atmospheric and Environmental Research Inc., Cambridge, Massachusetts.

Corresponding author address: Dr. Frank H. Ruggiero, AFRL/VSBE, 29 Randolph Road, Hanscom AFB, MA 01731-3010.
E-mail: ruggiero@arcdbs.plh.af.mil

sphere that a variety of meteorologically realistic profiles can yield the same brightness temperatures to within measurement error. Traditional processes to retrieve meteorological information from satellite sounders rely on iterative procedures that require an initial guess of the atmospheric thermodynamic profile (e.g., Hayden 1988). The guess can be generated from climatological data, upper-air analyses, or forecasts from a numerical weather prediction model.

Given the above problems in assimilating satellite sounder data into models, Lipton and Vonder Haar (1990a) developed a satellite–mesoscale model coupled approach. The coupled system works by using a mesoscale model to provide the first guess for the retrieval procedure. The deviations of the retrieved profiles of water vapor and ground temperatures from the first guess are then interpolated back to the model grid and the model values are adjusted accordingly. Next, the model is integrated for another period of time. The cycle of retrieval and model integration continues throughout the assimilation phase. The finescale vertical gradients from the model are retained while the broad-scale gradients are adjusted to match the observed radiance. There is some disagreement over the applicability of the coupled procedure (Thompson and Tripputi 1994). However, the technique has been successfully applied to the assimilation of ground temperatures and atmospheric water vapor for convective cases in eastern Colorado (Lipton and Vonder Haar 1990b), Texas (Lipton 1993), and Florida (Lipton et al. 1995) with generally favorable results. In addition, a similar approach has been implemented with global models and the Television Infrared Operational Satellite (TIROS) Operational Vertical Sounder (Gadd et al. 1995) with noticeable improvements to model forecasts.

Another method for assimilating satellite sounder information is four-dimensional variational analysis, which shows great promise (Andersson et al. 1994). In the variational approach the retrievals are obtained implicitly and there is no need to account for correlations between retrievals and background fields. However, this approach is computationally very expensive.

The objective of the research reported here is to implement and test the coupled technique of assimilating geostationary satellite sounder data in a mesoscale analysis and forecast system that is being developed jointly at the Air Force Research Laboratory (AFRL) and the Naval Research Laboratory (NRL). The forecast and analysis system is designed to run on a high-powered workstation that would be deployed at a local forecast office. For military applications, geostationary satellite sounders are important data sources since unavailability of ground-based observations is common in wartime tactical situations. Incorporating the coupled approach within the NRL/AFRL analysis and forecast system allows the satellite data to be merged with analyses from other data sources such as radiosondes and surface observations when available. A nonlinear vertical normal mode initialization (Sashegyi and Madala 1993) is used to damp out any spurious gravity waves that may be generated by assimilating temperature data into the prediction model. The inclusion of the initialization module allows for the assimilation of atmospheric temperature using the Lipton and Vonder Haar (1990a) technique. The implementation of the coupled technique in the NRL/AFRL mesoscale forecast and analysis system was evaluated for a midlatitude winter case during the Genesis of Atlantic Lows Experiment (GALE) as described below. The purpose is to investigate the applicability of the technique to a weather situation very different from the warm-season convective situations that had been the subjects of previous experiments in assimilation of geostationary sounder data.

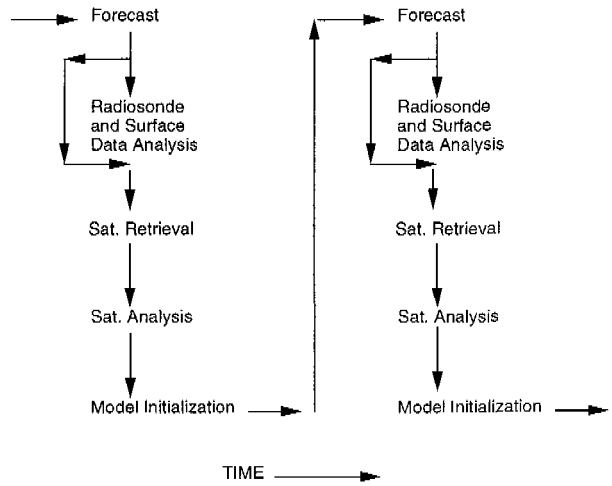

FIG. 1. Schematic showing the flow of the model–geostationary sounder coupled approach. Two analysis cycles are shown.

2. Coupled system

A schematic of the flow through the coupled model–geostationary sounder assimilation system is given in Fig. 1. Details of the individual modules are given below.

a. Radiosonde and surface data analysis

The objective analysis is accomplished by the successive correction scheme of Bratseth (1986) as adapted for upper-air data by Sashegyi et al. (1993) and surface data by Ruggiero et al. (1996). The main advantage to the Bratseth approach is that the analysis will converge to an optimum interpolation solution with less computer time and memory than does ordinary optimum interpolation. In addition, Carr et al. (1996) have shown the Bratseth scheme to be generally superior to the Barnes (1964) scheme and its subsequent variations (Barnes 1994a–c). The Bratseth technique avoids drawbacks of previous successive correction methods that converge to the observations excessively and give too much

weight to observations in data-dense regions (Carr et al. 1996). The degree of convergence of the analysis solution to the observations is controlled by an error parameter formulated under the assumption that the observational error is distributed randomly. The error parameter is defined as the ratio of the variance of the observation error to the variance of the background error. If the observations are assumed to be perfect, then the analysis will converge to the observations. A Gaussian function is used to model the background error horizontal spatial-correlation function employed by the analysis method. A correlation length scale is used that defines the halfwidth of the Gaussian function. This length scale is a function both of the data density and the scale of the features being resolved.

In this study, upper-air observations were analyzed on isobaric surfaces at every 50 mb from 100 to 1000 mb using a horizontal spatial resolution of 1.5° in latitude and longitude. Bogus soundings derived from operational Regional Analysis and Forecast System (RAFS) hemispheric analyses were added to fill in data-sparse regions over the ocean. The deviations from the first guess were then vertically interpolated back to the sigma surfaces. The surface data analysis, which is constructed on the model's lowest sigma layer, is univariate and has a horizontal grid resolution of 0.5° in latitude and longitude. Before the surface analysis begins, corrections are made to the observations to adjust for differences in the heights between the terrain on the model grid and the true terrain of the observations (Ruggiero et al. 1996). Sources of data for the surface analysis include regularly reporting hourly stations, Portable Automated Mesonet System stations deployed for GALE, and marine ship and buoy reports. The upper-air and surface data analyses are combined using a one-dimensional physical blending technique (Ruggiero et al. 1996).

b. *Satellite sounder data*

The geostationary sounder in operation during the 1986 GALE program was the VISSR Atmospheric Sounder (VAS) on board *GOES-6*. The VAS instrument has 12 infrared channels that can be used to estimate atmospheric temperature and water vapor concentrations as well as surface temperatures. More detailed information on the VAS instrumentation can be found in Menzel et al. (1983).

The retrieval of atmospheric profiles of temperature and water vapor mixing ratio from the VAS brightness temperatures follows the procedure outlined in Lipton and Vonder Haar (1990a). The procedure works in an iterative fashion by continuing to adjust the model's first-guess thermodynamic profiles and ground temperatures until brightness temperatures computed from them closely match the VAS observed brightness temperatures. The computed brightness temperatures are derived by computing atmospheric transmittances and integrating the radiative transfer equation. The atmospheric transmittances and radiative transfer integrals are computed using an efficient scheme based on empirical modeling (Smith et al. 1974; Weinreb and Neuendorffer 1973; McMillin and Fleming 1976; Fleming and McMillin 1977).

For this study, the VAS brightness temperatures were sorted, averaged, and earth-located by personnel at the National Oceanic and Atmospheric Administration/National Environmental Satellite, Data, and Information Service (NOAA/NESDIS). The VAS instrument can make measurements at a resolution as fine as 7 km. In order to compensate for data noise and to increase the accuracy of the soundings, boxes of 11 × 11 7-km pixels were averaged together (excluding cloudy pixels) to form a single set of 12 brightness temperatures to represent each box. In situations where an insufficient number of cloud-free pixels occurred in a box, the box was omitted from further processing. The NOAA/NESDIS cloud-clearing algorithm (Hayden 1988) was employed to identify cloudy pixels.

Objective analysis of thermodynamic profile increments (retrievals minus first guess) is similar to that mentioned above for the radiosonde data. Specifically, the analysis was performed using atmospheric temperature and relative humidity. Relative humidity is computed from the retrieved mixing ratios and temperatures. Modifications were made to the analysis procedure of Sashegyi et al. (1993) to take advantage of the high horizontal resolution of the VAS data. The analysis was performed on a horizontal grid with resolution of 0.25° lat–long. The vertical levels used for the analysis were chosen to coincide with the levels at which the retrieval software operates. While the retrieval software operates on 40 levels from 0.1 to 1000 mb, the analysis was performed on only the lowest 23 levels (to 70 mb). This choice of analysis levels eliminated vertical interpolation of the retrievals to the analysis levels, although interpolation to and from the model vertical (σ) coordinates was still needed. Care was taken to ensure that, in the course of the analysis, the method used to interpolate the background fields to the observation locations was exactly the same as the method used for generation of the first-guess profiles for the retrievals. To do otherwise would invite systematic errors to appear in the analyses.

One of the assumptions made by the Sashegyi et al. (1993) version of the Bratseth approach is that the observation error is random. Work with polar-orbiting atmospheric satellite sounders (Schlatter and Branstator 1979) indicates that this assumption is not valid for satellite sounder data. Therefore, the analysis method was altered for VAS applications to account for random and correlated parts of the observation error. Details of the modifications are given in the appendix.

To perform the modified analysis, one needs estimates of the random observation error variance (σ_ε^2), the spatially correlated observation error variance (σ_χ^2), the

background field error variance (σ_f^2), the length scale for the background correlation function (ρ), and the length scale for the observation error correlation (μ). The sources used for these parameters in the GALE case study are discussed in section 3.

c. *Model initialization*

The assimilation system uses nonlinear vertical normal-mode initialization, as described by Sashegyi and Madala (1993). The initialization procedure minimizes the time tendencies of the first three vertical (nonmeteorological) modes to reduce spurious oscillations associated with gravity waves. As described by Sashegyi and Madala (1993), the initialization is carried out without any boundary layer forcing or diabatic heating. A first-order closure mixing-length boundary layer package was subsequently added to the physical forcing in the initialization (Ruggiero et al. 1996).

d. *Forecast model*

The model used in this assimilation system is from the Navy's Operational Regional Atmospheric Prediction System (NORAPS) version 6 (Liou et al. 1994). This is the latest version of the model described by Madala et al. (1987), Hodur (1987), and Liou et al. (1990). NORAPS is currently run operationally by the U.S. Navy Fleet Numerical Meteorological and Oceanography Center for several areas of the world on a Cray C90 supercomputer. Work is under way to port a simplified configuration of the model to a high-performance RISC-type workstation with a computational performance of 30 Mflops. Initial tests have produced a 12-h model forecast in approximately 30 min of CPU time (Sashegyi et al. 1994).

NORAPS is a hydrostatic, primitive equation model written in flux form. The spatial finite difference equations are fourth-order accurate in the horizontal and second-order accurate in the vertical. Time integration is done using the efficient split-explicit scheme of Madala (1981). A Robert (1966) time filter is used to control high-frequency time oscillations. NORAPS contains a Kuo (1974) parameterization for deep convection and follows the approach of Tiedtke et al. (1988) for shallow convection. Large-scale precipitation is produced after the cumulus parameterization has been run by isobaric condensation in regions of supersaturation, following the procedure of Manabe et al. (1965). Precipitation falling into unsaturated layers is partially evaporated depending on how dry the unsaturated levels are. A multilevel planetary boundary layer is constructed using Monin–Obukhov (1954) similarity theory in the surface layer following Louis (1979) and turbulent vertical mixing above it. The mixing is accomplished by turbulent kinetic energy closure (Detering and Etling 1985). Surface temperatures are obtained by solving a surface energy budget using a two-layer force–restore method (Blackadar 1979). Atmospheric heating due to long- and shortwave radiation is updated every 15 min following the approach of Harshvardhan et al. (1987).

The horizontal grid is a staggered Arakawa C grid (Arakawa and Lamb 1977). The model can be triple nested. The lateral boundary time tendencies for the outer grid variables are relaxed toward interpolated global analysis and forecast time tendencies by the method of Perkey and Kreitzberg (1976). For the inner grids the values of the variables on the two grids are merged using the Davies (1976) method.

3. Case study

To examine the utility of the coupled analysis method for assimilating satellite atmospheric thermodynamic and surface temperature data in the NRL/AFRL assimilation system, experiments were conducted using data from the second Intensive Observation Period (IOP) of GALE (23–28 January 1986). Riordan (1990) and Doyle and Warner (1990) have detailed the synoptic- and mesoscale situations of the case. The case began as a cold-air damming event east of the Appalachian Mountains as surface high pressure moved eastward over eastern Canada. A coastal front formed over the west wall of the Gulf Stream between 1200 UTC 24 January and 0000 UTC 25 January 1986. The coastal front moved slowly west and eventually came onshore into eastern North Carolina. By 0000 UTC 26 January a small low formed along the coastal baroclinic zone just off the South Carolina coast and moved northward. This had the effect of pulling the coastal front back to the east along the North Carolina coast. The period 1200 UTC 24 January 1986 to 1200 UTC 25 January 1986 is highlighted here because of the availability of a large number of VAS retrievals on the 24th. Other days during the IOP did not have as many retrievals due either to the nonoperation of the sounder or extensive cloud cover. Meteorologically, the period chosen was important because it occurred during the beginning of cold-air damming and coastal front formation. Models that lack sufficient low-level vertical resolution will generally warm the near-surface layer excessively in these situations (Keeter et al. 1995).

A schematic illustrating the experiments is shown in Fig. 2. All experiments began with a 12-h model forecast valid at 1200 UTC 24 January 1986. This preliminary forecast was initialized from 2.5° RAFS analysis data and provides the initial background field for the 1200 UTC analyses.

Experiment 1 is considered a reference run, by which the other experiments were measured, and consisted of an 18-h assimilation run from 1200 UTC 24 January 1986 to 0600 UTC 25 January 1986. It was updated every 6 h with radiosonde and surface analyses. It assimilated all the available radiosonde data, including the special supplemental soundings that were taken during

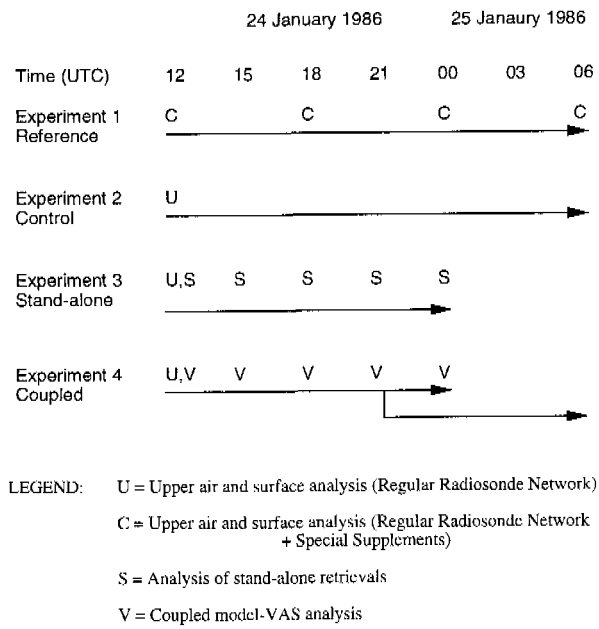

FIG. 2. Schematic depicting the data analysis and forecast durations for each of the four experiments.

GALE. The analyses generated at the 6-h intervals were used to verify the subsequent experiments.

Experiment 2 is a control run. In it, the model was integrated without assimilation for 18 h to 0600 UTC 25 January. The control run was initialized at 1200 UTC 24 January 1986 with radiosonde and surface data; however, it did not include the special GALE soundings. This run was chosen to represent the analysis and forecast information that is typically available to the operational forecaster.

Experiment 3 is the stand-alone retrieval assimilation run. Personnel from NOAA/NESDIS in Madison, Wisconsin, computed the retrievals for this run independent of the NORAPS model. The retrievals for this study were generated from the archived 3-hourly brightness temperatures using the retrieval method (Hayden 1988) operational in 1994 (G. Wade 1994, personal communication). In this method, 6-, 12-, and 18-h National Meteorological Center (now known as the National Centers for Environmental Prediction) operational RAFS forecasts were interpolated in time to provide the first guess for generating these retrievals (Hayden et al. 1996). For the stand-alone retrieval assimilation, the retrievals were assimilated into the model at 3-h intervals beginning at 1200 UTC 24 January. The coverage afforded by the VAS retrievals can be seen in Fig. 3. For the assimilation at 1200 UTC 24 January 1986, the background field used for the analysis was the analysis of radiosonde and surface data that was constructed for the control experiment. For the next 12 h, a 3-h cycle of model integration and VAS data assimilation was carried out. In this experiment the retrieved surface temperatures were not assimilated. The inclusion of the stand-alone retrievals was not carried out to evaluate the quality of the operational retrievals. A single case study is insufficient for such an evaluation. Rather, it provides an additional insight into the behavior of the satellite data objective analysis by showing how it performs with different methods of handling the retrieval process.

Experiment 4 is the coupled system run that assimilated VAS brightness temperature data by the means illustrated in Fig. 1. It is essentially the same as experiment 3 except that all the VAS retrievals were generated using, as the first-guess profile, the same NORAPS forecast that forms the background field for the analysis. In addition, the model was run in forecast mode for 9 h from 2100 UTC 24 January to 0600 UTC 25 January. The purpose of this model run was to simulate an operational scenario where a forecast is needed to begin running prior to the availability of the 0000 UTC soundings. For the coupled run, it was not possible to rely solely on the model for supplying first-guess data for the retrievals, since the model top was at an insufficient altitude for the necessary radiative transfer computations. The model provided first-guess data up to the 60-mb level. From 50 to 10 mb, interpolated values from the High Resolution Analysis System (HIRAS) prepared by the Air Force Global Weather Center were used. Above 10 mb the temperature profile from the rocketsonde launched at Cape Canaveral at 1600 UTC 24 January 1986 was used. Several profiles were examined to ensure that no spurious lapse rates were introduced into the profiles when switching from the HIRAS analysis to rocketsonde data above 10 mb. It is possible, however, that discontinuities could exist between the top of the model forecast and the HIRAS data. To help mitigate this problem a linear blending between the model and the HIRAS data was performed between 70 and 50 mb. Examples of the resulting first guess profiles are shown in Fig. 4. The profiles through the transition zones at 70–50 mb and 10–7 mb are relatively smooth and show no evidence of any significant inconsistencies among the datasets. However, our confidence in the profiles above 100 mb is limited by the absence of independent ground truth data.

In addition to the atmospheric thermodynamic data, the retrieved surface temperatures were also assimilated into the model. The surface temperature assimilation must be carried out in a continuous manner to retain the desired features since they can change rapidly and must be modeled smoothly. For this experiment the original surface temperature coupling procedure of Lipton and Vonder Haar (1990a) was modified in order to facilitate its implementation into the NRL/AFRL analysis system. At the assimilation starting time (1200 UTC 24 January 1986) surface temperature retrievals were calculated for each of the VAS assimilation times (1200, 1500, 1800, 2100, 0000 UTC). This was performed using the VAS brightness temperatures for those times with the 1200 UTC 24 January background analysis

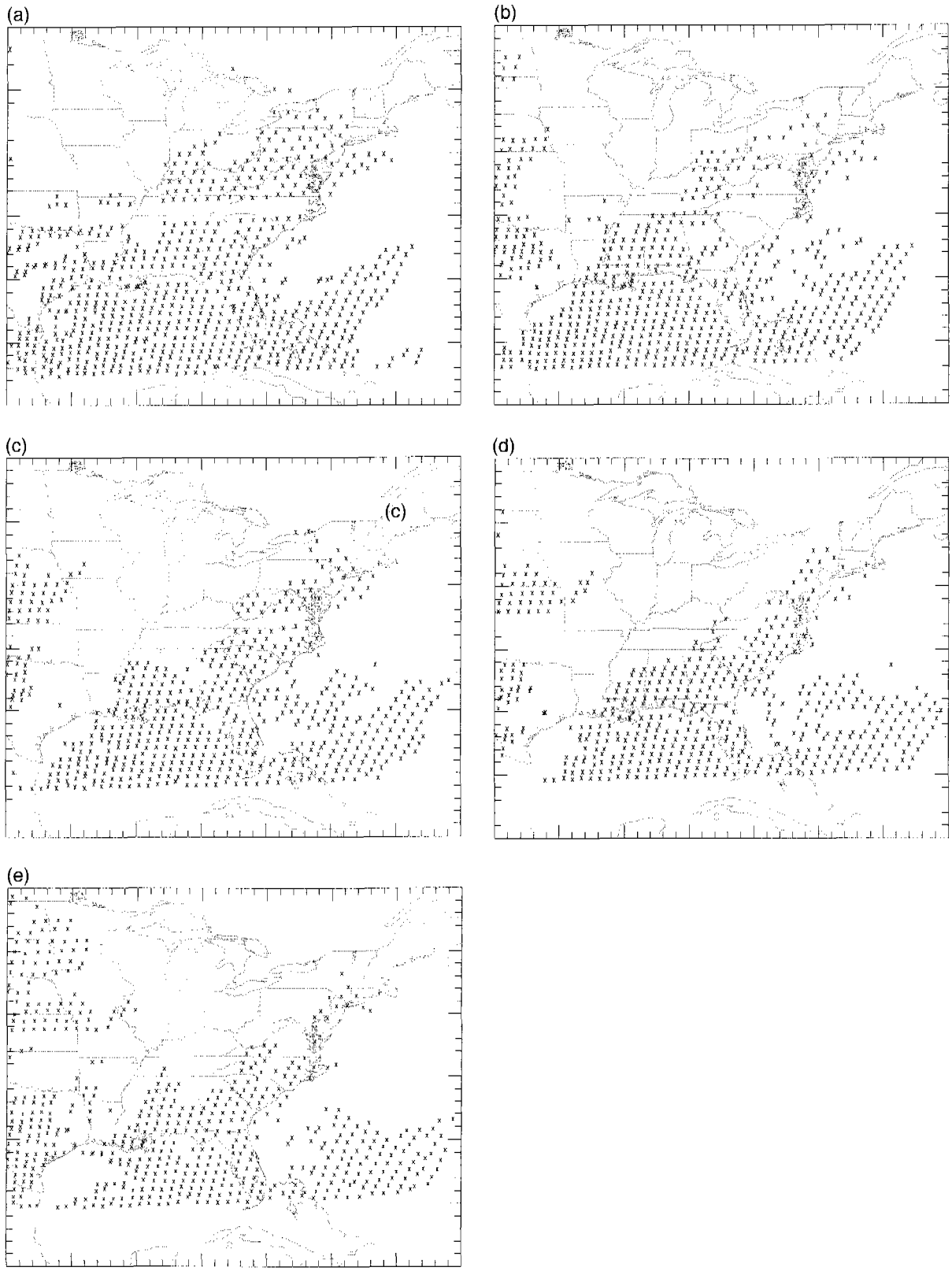

FIG. 3. VAS retrieval locations for (a) 1200 UTC 24 Jan 1986, (b) 1500 UTC 24 Jan 1986, (c) 1800 UTC 24 Jan 1986, (d) 2100 UTC 24 Jan 1986, and (e) 0000 UTC 25 Jan 1986.

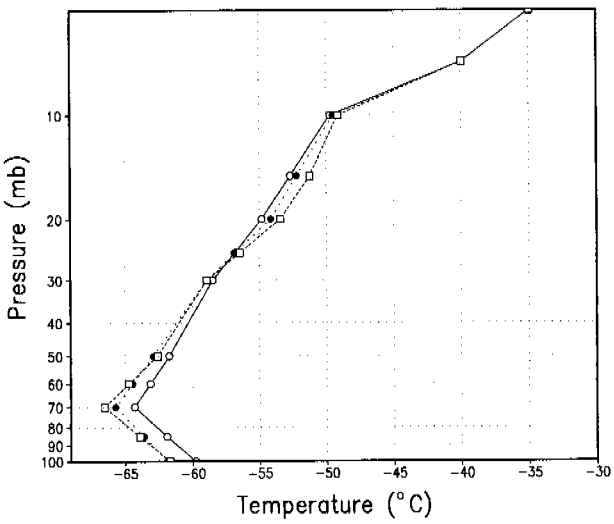

FIG. 4. Examples of temperature profiles used as first guesses for VAS retrievals from 100 to 5 mb. The solid line with hollow circles is for a retrieval located near Greensboro, NC (36.08°N, 79.95°W), at 1200 UTC 24 Jan 1986. The dotted line with solid circles is for a retrieval located near Fayetteville, NC (35.03°N, 78.72°W), at 1800 UTC 24 Jan 1986. The dashed line with hollow squares is for a retrieval located near Columbia, SC (33.85°N, 80.32°W), at 0000 UTC 25 Jan 1986.

fields as the first guess for the retrievals. The surface temperature retrievals at each time were then objectively analyzed using the procedure in section 2. After completing the analyses, temporal interpolation spline parameters were computed for the surface temperatures at each grid point. The spline parameters were then included as input to the model so that updated surface temperatures were available at every time step. These updated temperatures were then used to nudge the model-computed surface temperatures following the procedure of Stauffer and Seaman (1990). A temporal weighting factor on the satellite surface temperature data was linearly interpolated from zero to one over the first 3 h of assimilation to ensure a smooth transition from model- to satellite-derived surface temperatures. A relatively large nudging factor of 0.003 was used to make the model output surface temperatures highly responsive to the retrievals.

The analysis of the VAS retrieval data was run on a single grid with a domain from 10.0° to 60.5°N and 115.5° to 44.5°W and a resolution of 0.25° lat and long. After the analysis was completed, the analysis increments were vertically and horizontally interpolated to the model grid. The model was run in triple nested mode with the domains of the three grids depicted in Fig. 5. The horizontal resolution of the outermost grid was 1.5° lat by 2.0° long. For each succeeding inner grid the horizontal spacing decreased by a factor of 3 such that for the innermost grid the spacing was approximately 18 km at 35°N. The model was run with 16 vertical σ layers ($\sigma = p/p_s$), where p is pressure and p_s is the surface pressure. The vertical distribution of the layers, given in Table 1, is such that four of the model layers were located in the lowest ~500 m of the atmosphere. The lateral boundaries of the outermost grid were updated using interpolated RAFS analysis tendencies.

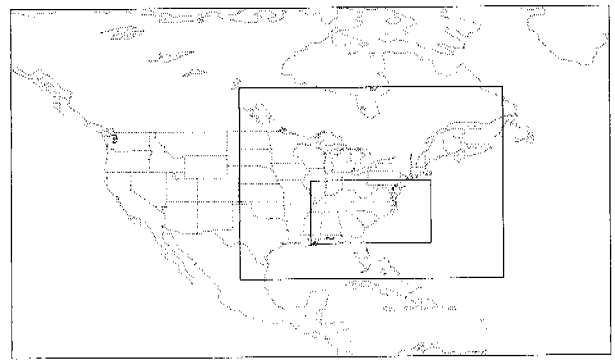

FIG. 5. Domains of the three nested NORAPS model horizontal grids used in this study.

In performing the radiosonde and surface data analyses, the background error and forecast error growth rates were taken to be the same as used respectively by Sashegyi et al. (1993) and Ruggiero et al. (1996). Background error correlation length scales of 600 km for the radiosonde data analysis and 300 km for the surface data analysis were used. For the VAS analyses, the correlation length scale of the background error was set at 600 km. The value of 600 km was chosen to keep it consistent with what was used for the radiosonde data analysis. A value of 500 km was used for the correlation length scale of the observation error in the VAS retrieval analysis. This value was chosen based on the work of Schlatter and Branstator (1979) in their study of error associated with the *Nimbus-6* sounder.

Selection of the observation error values for the retrievals was challenging. To the authors' knowledge, the only published values of observation error from satellite

TABLE 1. Vertical distribution of the 16 σ levels for the NORAPS model configuration used in this study.

Level	σ
1	0.0500
2	0.1500
3	0.2500
4	0.3500
5	0.4500
6	0.5500
7	0.6500
8	0.7475
9	0.8250
10	0.8750
11	0.9100
12	0.9375
13	0.9600
14	0.9775
15	0.9900
16	0.9975

sounders are in Parrish and Derber (1992), for polar-orbiting sounders in association with a global model. The observation error values given by Parrish and Derber (1992) were for temperature only. We could find no published substantiation of the values. On the basis of the values given by Parrish and Derber (1992), an observation error of 3.6° for the VAS temperature retrievals at all levels was used. The partition of the observation error between random and correlated error was accomplished by sensitivity studies to see how much the observation error needed to be considered correlated to reduce the mean bias in the retrievals to near zero. This resulted in values of 3.5° for the random observation error and 1° for the spatially correlated observation error standard deviations. Likewise, for relative humidity, random and spatially correlated standard deviations of 15% and 25%, respectively, were chosen.

Another problem that needed to be addressed was the specification of the background error for the analysis. The background error at a given time can be thought of as the analysis error from the previous analysis time, plus some error growth that occurs during the model integration between the two analysis times. In previous work, Sashegyi et al. (1993) approximated the background error by using a radiosonde observation error estimate in place of the previous analysis error and adding to it an error growth rate multiplied by the length of time between analyses. The substitution of the observation error for the analysis error was made because no straightforward method of computing an analysis error for the Bratseth scheme currently exists. However, in an optimal interpolation scheme, the analysis error must be less than or equal to the smaller of the observation error and the background error (Daley 1991). For this study, the background error was taken to be equal to the smaller value; that is, it was taken as the upper limit of the principle cited by Daley allows. Applying this principle at 1200 UTC 24 January, the analysis error must be less than the error of the more accurate of the two data sources (radiosonde and VAS) that were analyzed in sequence. For analysis times beyond 1200 UTC 24 January, an approximation of the background error was accomplished by using the radiosonde observation error plus the forecast error growth from 1200 UTC 24 January to the later analysis time. This approach was used because, even with compounding growth, it yielded error values smaller than the VAS observation error. Using the higher VAS observation error would have implied that the VAS data would make the analysis worse. The current approximation makes the conservative assumption that the VAS data have no negative impact on the analysis statistics error during the assimilation period.

The VAS retrievals were accomplished using all the channels with the exception of channels 6, 11, and 12. Channel 11 was not operational at the time and channels 6 and 12 were omitted since they are sensitive to solar radiation and substantial errors can be introduced trying to quantify the solar radiation effect.

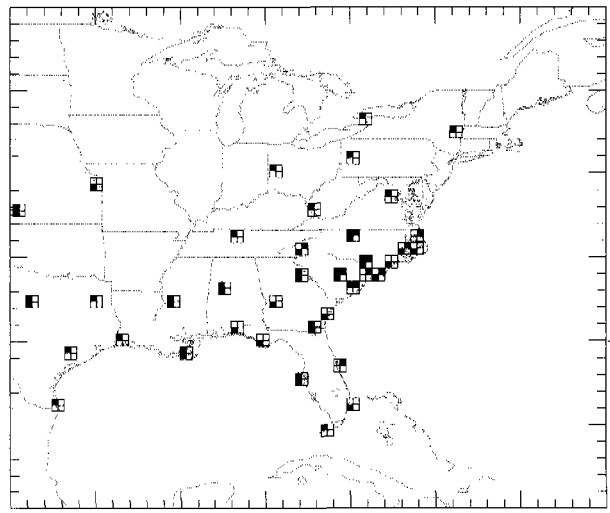

FIG. 6. Radiosonde station locations that were used for analysis comparisons. A solid top-left quadrant indicates the location was used for comparisons at 1200 UTC 24 Jan, a solid top-right quadrant indicates the location was used for comparisons at 1800 UTC 24 Jan, and a solid bottom-left quadrant indicates the location was used for comparisons at 0000 UTC 25 Jan.

4. Results

Retrievals, analyses, and forecasts were compared for selected points within the analysis domain where assimilated retrievals and reference run radiosonde observations were nearly coincident. The locations of the radiosonde stations used in the comparisons are shown in Fig. 6. At each time, retrievals, analyses, and/or forecasts were compared with the reference run analyses. The reason the reference run analysis was chosen as the standard of comparison and not the actual radiosonde sounding was to lessen the impact of the radiosonde observation error. Analysis locations near radiosondes were chosen because, in theory, those points should be the most accurate source of data. For each comparison with the reference analysis, root-mean-square (rms) errors were computed.

a. Comparison of coupled and stand-alone retrievals

There were three times during the case study period when radiosonde observations were available along with VAS retrievals. A comparison of the rms temperature errors of the coupled and stand-alone retrievals at 1200 and 1800 UTC 24 January 1986 and 0000 UTC 25 January 1986 is shown in Fig. 7. In general, the coupled retrievals are superior to the stand-alone retrievals. Particularly at levels below 800 mb, the coupled approach has substantially reduced the errors in the retrieved temperatures compared to the stand-alone retrievals. At all

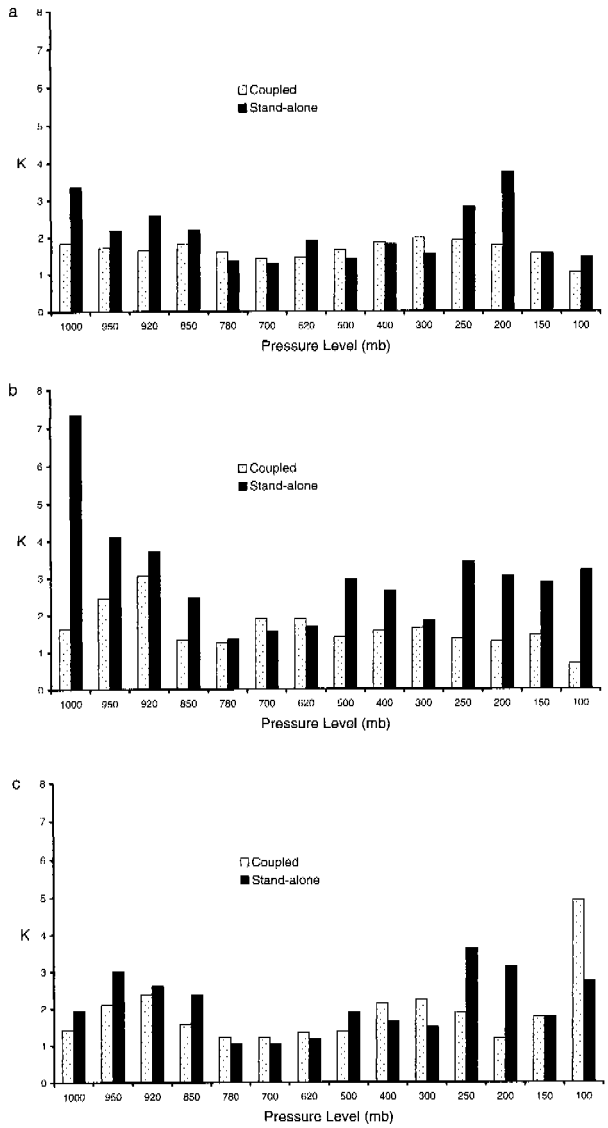

FIG. 7. Rms errors of temperature from the coupled and stand-alone retrievals relative to the reference run at locations that have nearly coincident radiosonde soundings and retrievals at (a) 1200 UTC 24 Jan 1986, (b) 1800 UTC 24 Jan 1986, and (c) 0000 UTC 25 Jan 1986.

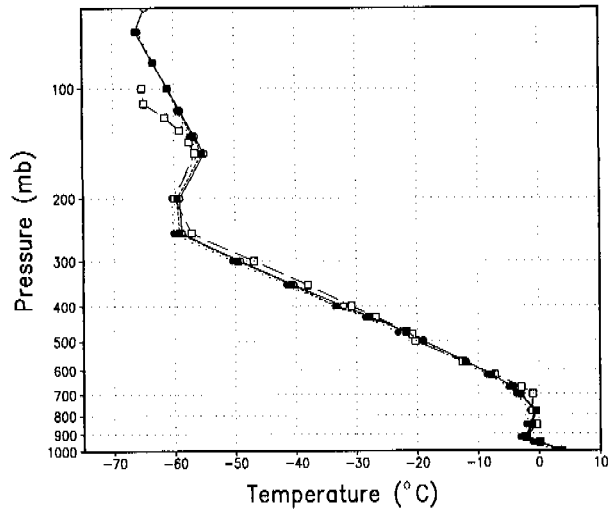

FIG. 8. Temperature profiles for first guess (solid line, hollow circles), coupled retrieval (dotted line, solid circles), resulting coupled analysis (short-dashed line, solid squares), and radiosonde (long-dashed line, hollow squares). Profiles are located near Fayetteville, NC, at 0000 UTC 25 Jan 1986.

three times, the stand-alone retrievals are slightly better at some of the levels around the midtroposphere. The magnitude of the difference of the two retrievals at these levels is small enough not to be of any real concern. One level and time at which the stand-alone retrieval is substantially better than the coupled retrieval is at 100 mb on 0000 UTC 25 January 1986. It is believed that the source of this problem is errors from the NORAPS forecast model. C.-S. Liou (1995, personal communication) has suggested that the NORAPS model may not be as accurate in the stratosphere as it is in the troposphere. An example of the problem caused by this can be seen in Fig. 8. Four different temperature profiles are presented for a single retrieval location. The profiles correspond to the first guess, the coupled retrieval, the resulting coupled analysis, and a nearly collocated radiosonde observation at 0000 UTC 25 January 1986. Up to 150 mb, the profiles are in general agreement to within expected error; however, while the first guess, coupled retrieval, and coupled analysis profiles are all close together near 100 mb, the radiosonde profile is substantially cooler at that level. The error at that level clearly can be attributed to the first guess. At 100 mb the retrieval and analysis steps did nothing to enlarge nor correct the first-guess error. Likewise, inspection of the four profiles at other radiosonde observations times (1200 and 1800 UTC) indicates that no substantial errors were introduced by the coupled retrievals or coupled analysis.

In Fig. 9 the rms errors of relative humidity for the three comparison times are given. As with the temperature analyses, the coupled retrievals are generally better than the stand-alone retrievals. Again there are exceptions. For example, the coupled retrieval is substantially worse than the stand-alone retrieval at 1000 mb for both times at 1200 UTC 24 January 1986 and 0000 UTC 25 January 1986. Looking at the evolution of the relative humidity rms errors over time, one can see that the stand-alone retrieval is better at half of the levels presented at 1800 UTC. However, by 0000 UTC 25 January 1986 the coupled retrievals are better at all but two levels. This is indicative of the beneficial aspect of the coupling procedure where one would expect the coupled retrievals, making use of improving first guess profiles as the assimilation proceeds, to improve over time relative to the stand-alone retrievals.

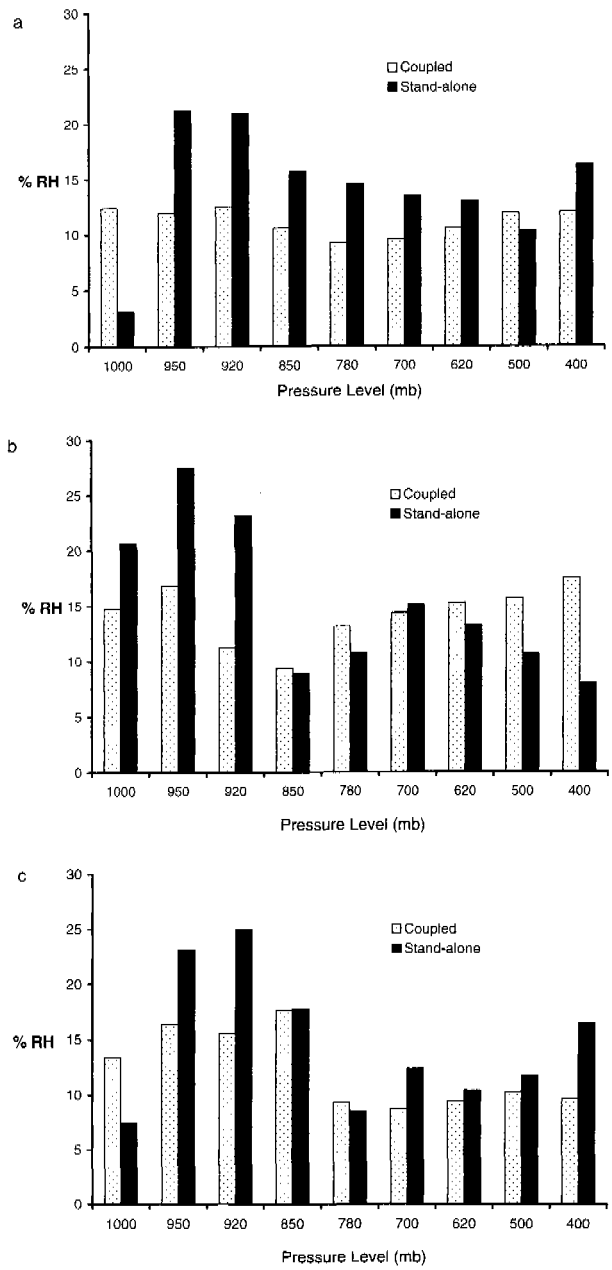

FIG. 9. Rms errors of relative humidity from the coupled and stand-alone retrievals relative to the reference run at locations that have nearly coincident radiosonde soundings and retrievals at (a) 1200 UTC 24 Jan 1986, (b) 1800 UTC 24 Jan 1986, and (c) 0000 UTC 25 Jan 1986.

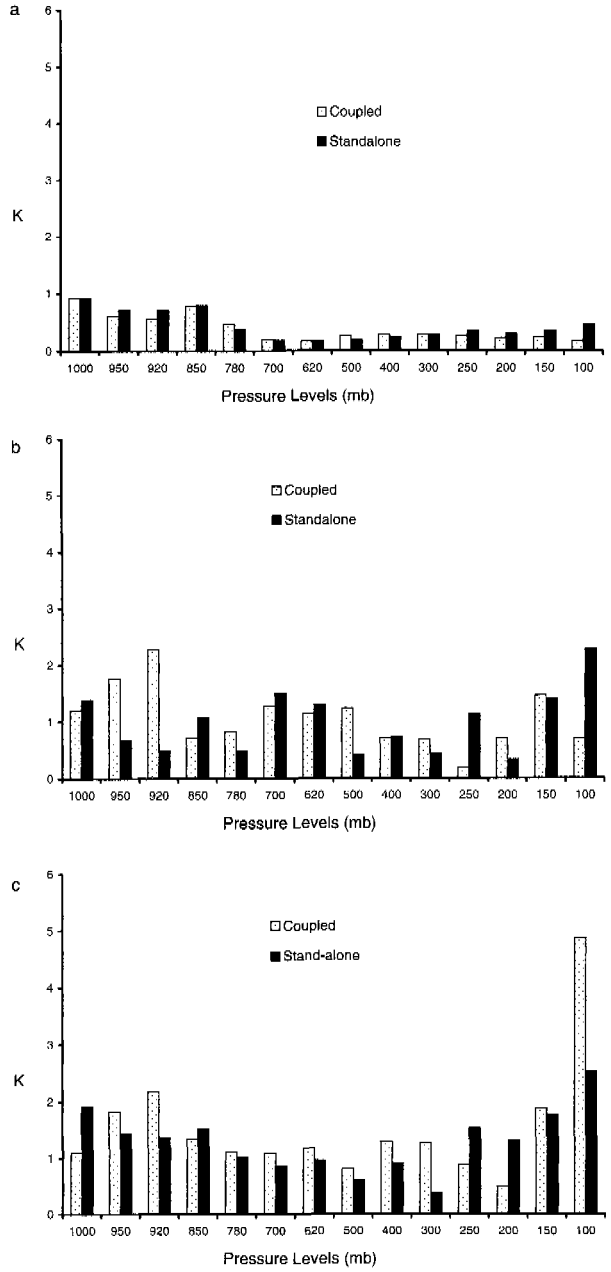

FIG. 10. Rms errors of temperature from the coupled and stand-alone analyses relative to reference run at location that have nearly coincident radiosonde soundings and retrievals at (a) 1200 UTC 24 Jan 1986, (b) 1800 UTC 24 Jan 1986, and (c) 0000 UTC 25 Jan 1986.

b. Comparison of coupled and stand-alone analyses

Using the same locations as above, the resulting analyses from the stand-alone and coupled runs were compared. The results for temperature are in Fig. 10. The interesting point here is that, while the retrievals input to the analyses were generally better for the coupled case than the stand-alone case, the resulting analyses for the stand-alone runs are slightly better on average than the coupled analyses. One possible reason for this contrast is that the stand-alone retrieval errors are more independent of the analysis background than are the coupled retrievals. At present, no account is made for the correlation of the background errors with the observations. The end result is that observation errors are possibly being canceled out more efficiently in the stand-alone analysis than in the coupled analysis. In-

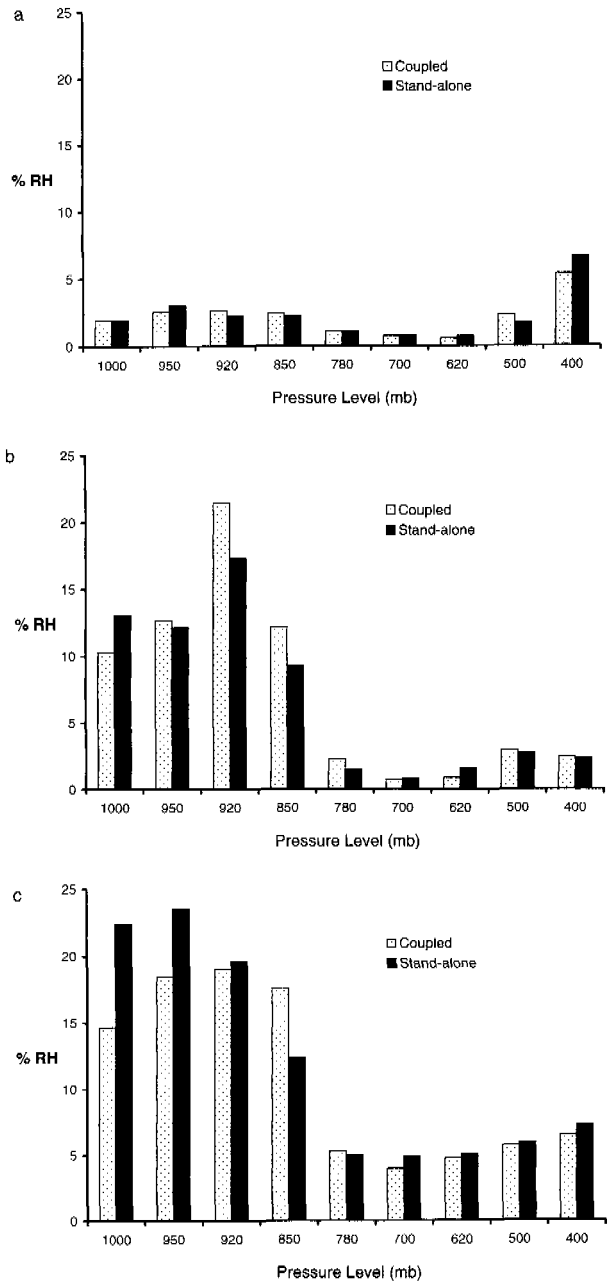

FIG. 11. Rms errors of relative humidity from the coupled and stand-alone analyses relative to the reference run at locations that have nearly coincident radiosonde soundings and retrievals at (a) 1200 UTC 24 Jan 1986, (b) 1800 UTC 24 Jan 1986, and (c) 0000 UTC 25 Jan 1986.

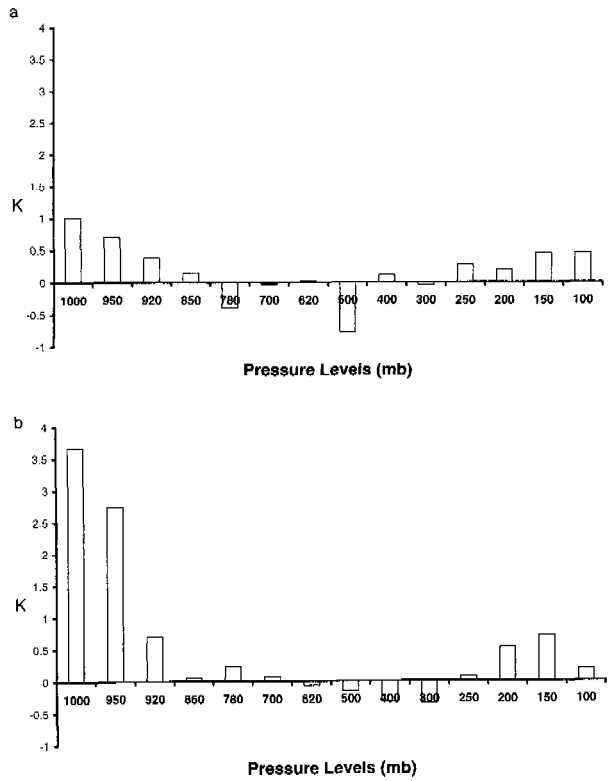

FIG. 12. Rms temperature error differences of coupled run from control run at (a) 1800 UTC 24 Jan 1986 and (b) 0000 UTC 25 Jan 1986.

deed, Thompson and Tripputi (1994) pointed out the potential for this problem. A particular example for this can be seen in looking at the rms errors at 100 mb noted in the previous section. Any errors or biases in the forecasts at this level are negatively impacting the accuracy of the retrievals. In addition, the coupled procedure using the retrieval error modeled as a constant with height is clearly an oversimplification. A four-dimensional variational approach would avoid some of these problems.

The comparisons for the coupled and stand-alone analyses of relative humidity are given in Fig. 11. At the lower levels the coupled analyses improve relative to stand-alone analyses as the assimilation cycles progress. At around 850 mb, the stand-alone analyses of relative humidity are better than the coupled analyses. At the upper-tropospheric level the coupled analyses are better. Again, we believe that the chief explanation for the levels where the stand-alone analyses are better than the coupled analyses is that the analysis does not account for the correlation of the background and observation errors.

c. *Comparison of the coupled analyses with the control run*

Figures 12 and 13 show the difference between the control run and coupled run analysis rms errors for temperature and relative humidity, respectively. Positive values indicate that the coupled run analysis is an improvement over the control run forecasts. The comparisons are performed at 1800 UTC 24 January and 0000 UTC 25 January 1986 for locations where radiosondes and retrievals are nearly coincident. For both variables, the coupled run is superior to the control run at most

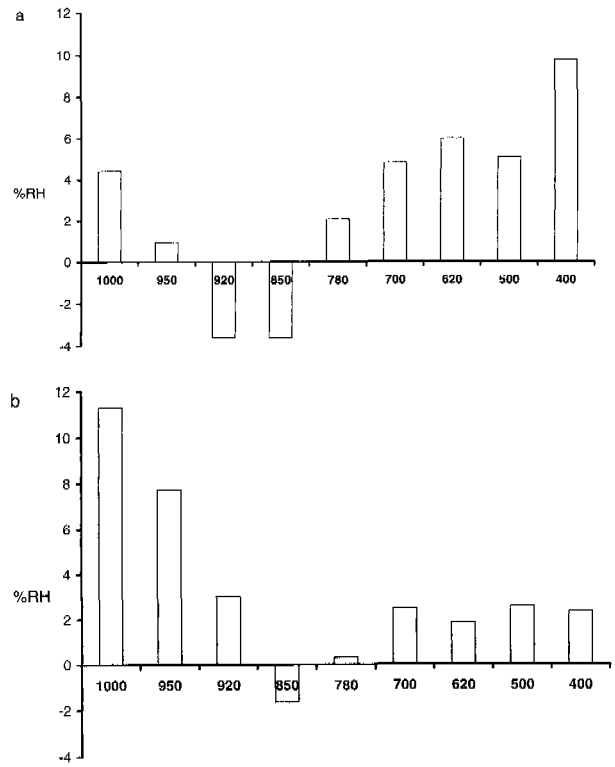

FIG. 13. Rms relative humidity error differences of coupled run from control run at (a) 1800 UTC 24 Jan 1986 and (b) 0000 UTC 25 Jan 1986.

levels. In addition, the magnitude of the difference at those levels where the control run is better decreases with time. The amount of improvement at the levels where the coupled run is better increases with time and is of a much larger magnitude than the difference where the control run is better.

As mentioned in the introduction, one of the objectives of this research was to assess the applicability of using the coupled procedure in a wintertime situation. Within the assimilation phase, the coupled procedure did produce improved analyses compared to the control run. A comparison of the surface temperatures for the reference, control, and coupled runs is given in Fig. 14. In the reference run, the thermal gradient associated with the land–sea boundary is clearly evident. The cold-air pool between the coastal front and the Appalachian Mountains was not as cold at this point as it became later in the period. The coupled and control runs both show a strong thermal gradient associated with the coastal front. However, the control run is cooler than the reference run for the area between the coastal front and Appalachian Mountains, while the coupled run is warmer in this area. During this time this area had relatively little cloud coverage so the reference run surface temperatures were reacting to the midday solar heating. Experience with the forecast model by the authors has shown that its surface energy budget has trouble properly producing sufficient amplitude in the diurnal heating cycle, as is evident here. This model deficiency could be due in part to the relatively simple soil parameterization used in the model and/or the inadequacy of

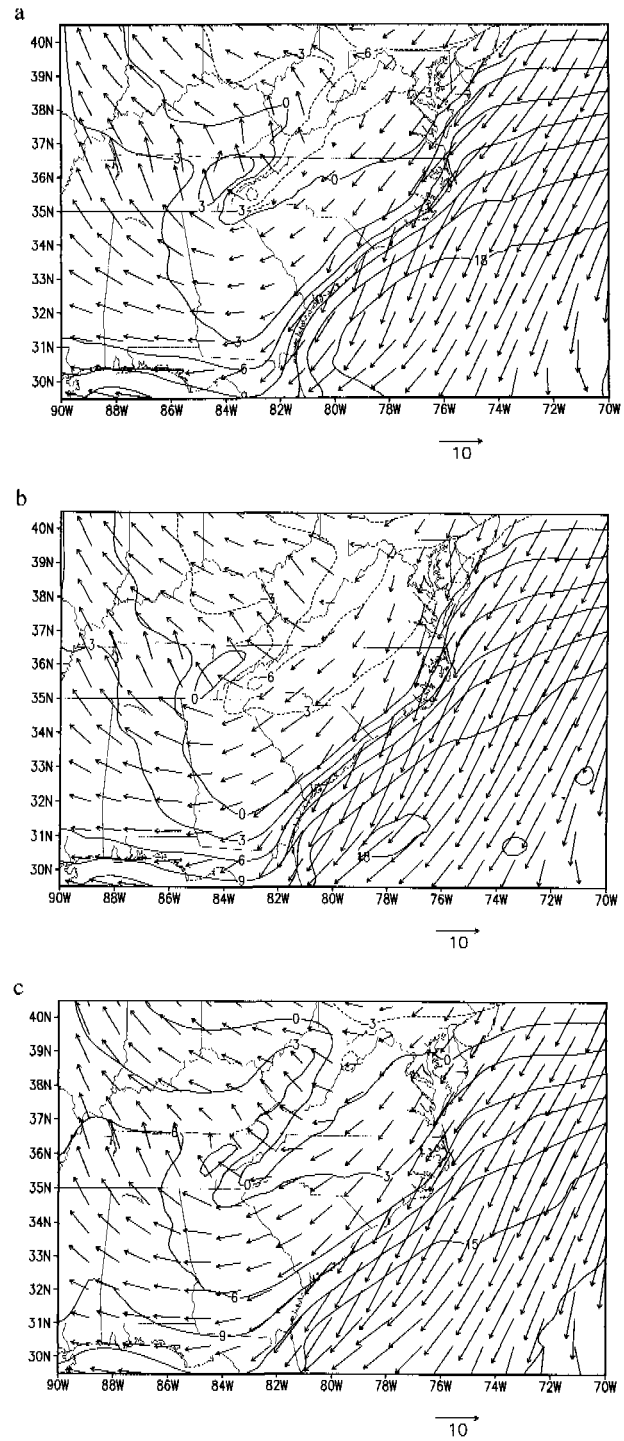

FIG. 14. Surface layer temperature (isotherms every 3°C) and wind vectors (m s^{-1}) fields for (a) reference run, (b) control run, and (c) coupled run at 1800 UTC 24 Jan 1986.

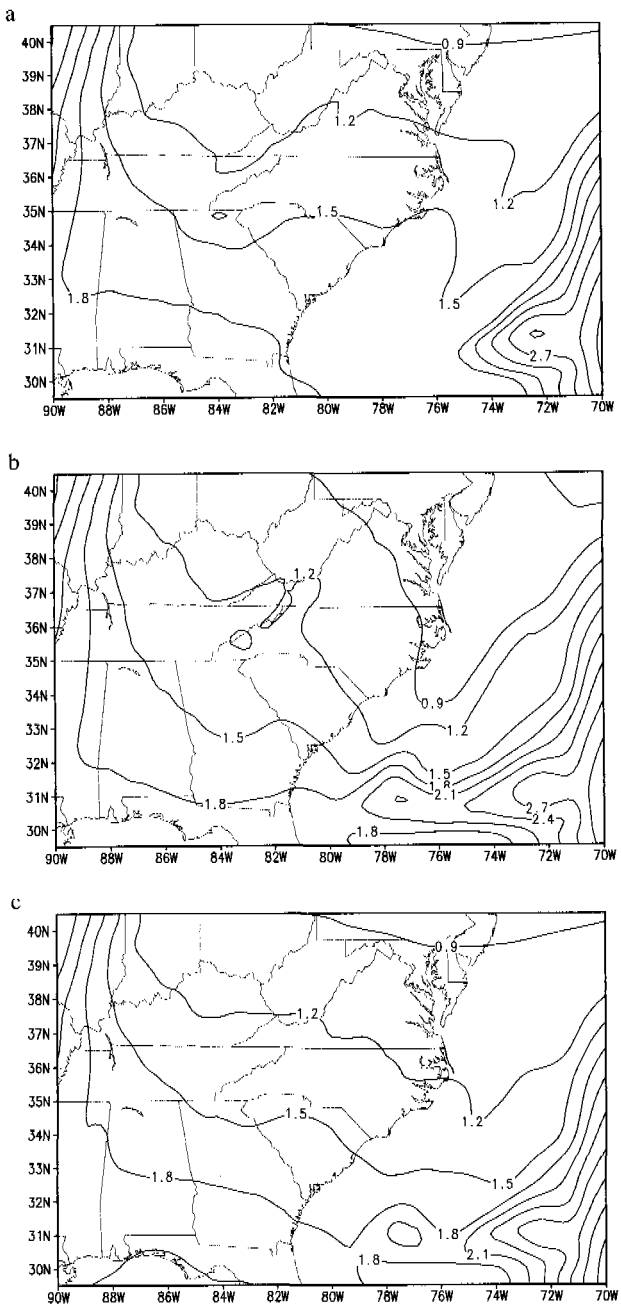

FIG. 15. Mixing ratio (contours every 0.3 g kg^{-3}) at 700-mb level for (a) reference run, (b) control run, and (c) coupled run at 1800 UTC 24 Jan 1986.

the input surface characteristics that affect the model's surface energy budget. Although the coupled analysis overcompensates for this model deficiency, it is closer than the control run. The assimilation of the satellite-derived surface temperature is important here. In preliminary runs of the coupled procedure without assimilating surface temperatures, the coupled run showed very little difference from the control run at this level.

Figure 15 shows the mixing ratios for the reference, control, and coupled runs at 700 mb. In this case, the coupled run is closer to the reference run than the control run is in showing the correct moisture amounts in the area where the cold-air dome developed (between the Carolina coast and the Appalachian Mountains). The coupled run showed higher amounts of water vapor at this level than did the control run. This difference can be important in the development of the cold-air dome and in strengthening the coastal front even though the moisture difference occurred at a height above the vertical extent of both features. Bell and Bosart (1988) have found that precipitation aloft and evaporative cooling below are important mechanisms for establishing and maintaining the cold-air dome.

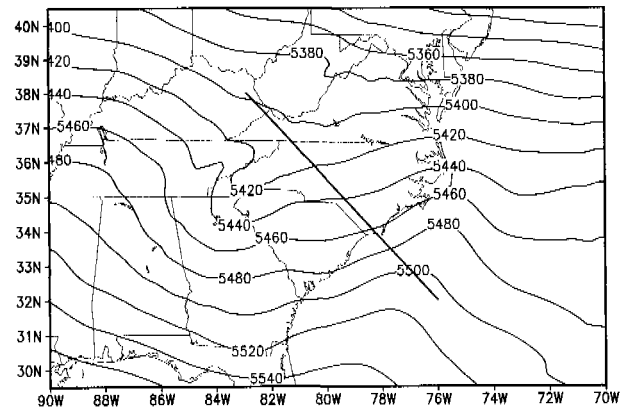

FIG. 16. Thickness of 1000–500-mb layer (contours every 20 m) for the reference run at 1800 UTC 24 Jan 1986. Solid line indicates location of a cross section to be presented in later figures.

In Fig. 16 the 1000–500-mb thickness field is presented for the reference run at 1800 UTC 24 January 1986. The thickness lines are generally zonal with warm-air ridging off the Carolina coast in the vicinity of the Gulf Stream. Figure 17 depicts the improvement

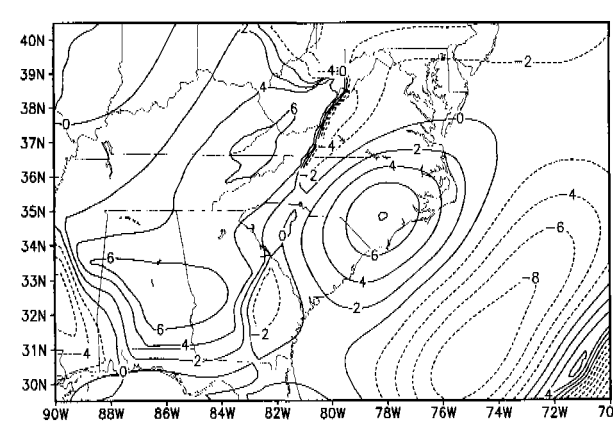

FIG. 17. Difference of errors in the 1000–500-mb layer thickness (contours every 2 m) for the background and analysis at 1800 UTC 24 Jan 1986 for the coupled experiment. Values are positive where the analysis was an improvement over the background. Errors are relative to the reference run.

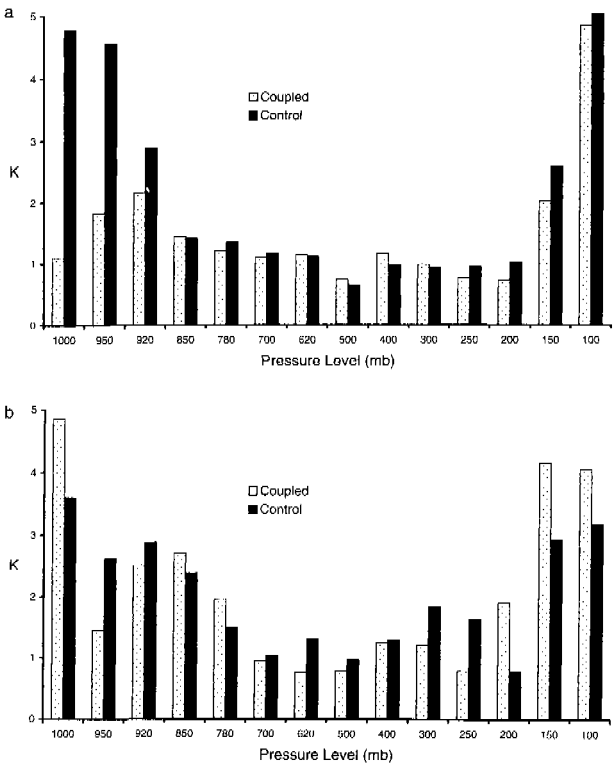

FIG. 18. Rms errors of temperature from the coupled and control run forecasts relative to the reference run at (a) 0000 UTC 25 Jan 1986 and (b) 0600 UTC 25 Jan 1986.

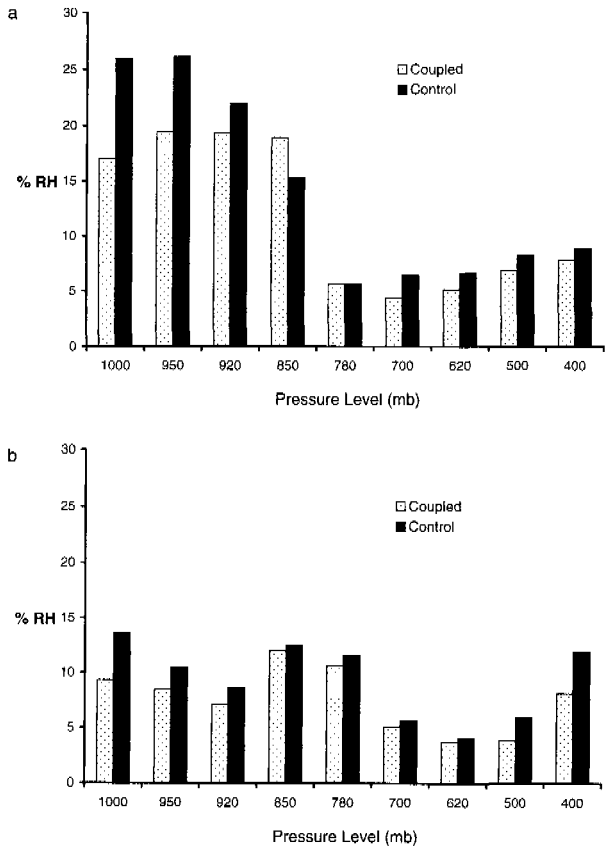

FIG. 19. Rms errors of relative humidity from the coupled and control run forecasts relative to the reference run at (a) 0000 UTC 25 Jan 1986 and (b) 0600 UTC 25 Jan 1986.

of the thickness field that resulted from the 1800 UTC retrieval and analysis steps. Positive values indicate areas where the analysis improved over the background (3-h forecast). Over land areas the assimilation displays widespread improvement particularly in the eastern portions of the Carolinas and central Alabama. The primary area where the analysis is not as close to the reference is over the Atlantic Ocean. Given the absence of data over the ocean for this time, the reference run is not as trustworthy over the ocean. While the assimilation of the coupled retrievals does improve the analysis, the magnitude of the improvement is relatively small. This is due to the large errors attributed to the retrievals in the statistics that govern the behavior of the analysis.

d. Comparison of the coupled and control run forecasts

In order to provide a test of the operational applicability of the coupled system to provide improved short-term forecasts, a comparison was made between the coupled and control run forecasts. The coupled forecast run assimilated VAS thermodynamic data up to and including 2100 UTC 24 January 1986 and the control run forecast started with the last available radiosonde data at 1200 UTC 24 January 1986. The forecasts were evaluated at 0000 and 0600 UTC 25 January 1986. The comparisons of rms errors for temperature at each time are given in Fig. 18. At most of the levels the coupled forecasts of temperature are similar to the control forecasts at 0000 UTC. The notable exception is at the lower levels (1000–920 mb) where the coupled run is significantly better than the control run. The main reason for the improvement of the coupled run at the low levels is the model's insufficient diurnal amplitude of the surface temperatures. Since the coupled run has updated the temperatures during the 1200–2100 UTC assimilation phase, it has been able to overcome this problem. At 0600 UTC the control run compares more favorably to the coupled forecasts. In particular, the control run is better at 1000 mb and at and above 200 mb. As mentioned earlier, the model appears to be relatively inaccurate with respect to temperature above the tropopause and the coupling procedure may have exacerbated the problem slightly. The rms errors for the relative humidity forecasts are shown in Fig 19. In this case the coupled run shows uniform and consistent improvement over the control run forecasts. By 0600 UTC 25 January 1986, the coupled forecast has better relative humidity statistics than the control run at all levels.

A more subjective evaluation of the quality of the

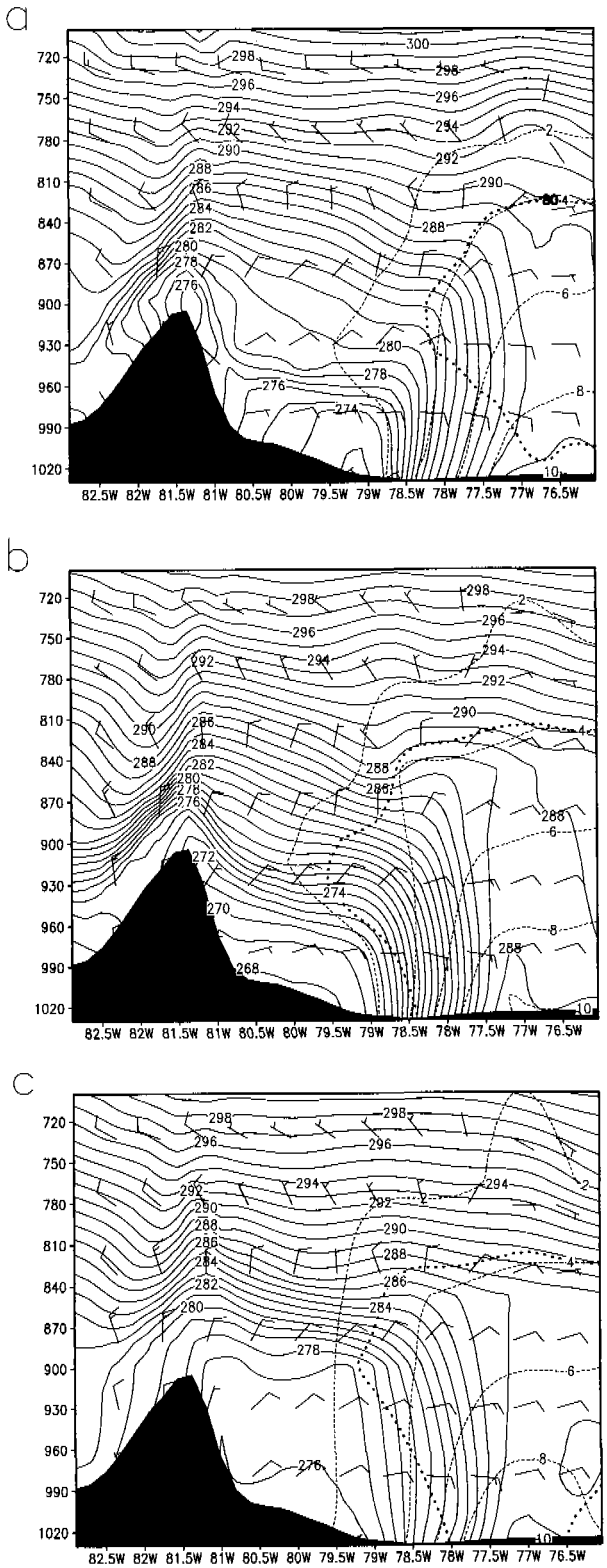

FIG. 20. Vertical cross section corresponding to line drawn in Fig. 16 for (a) reference run, (b) control run, and (c) coupled run forecast valid at 0000 UTC 25 Jan 1986. Potential temperature is depicted by the solid lines (contoured every K), specific humidity is shown by the dashed lines (contoured every 2 g kg^{-1}), the wind barbs are for the horizontal wind with each whole flag representing 5 m s^{-1}, and the 80% relative humidity contour is depicted by the heavy dotted line.

forecasts can be achieved by looking at a cross section that is approximately normal to the coastal front. In Fig. 20 cross sections that correspond to the line drawn in Fig. 16 are presented. The cross sections correspond to the reference run analysis and control and coupled run forecasts valid at 0000 UTC 25 January 1986. All three runs depict in varying degrees the cold-air damming and coastal thermal gradient. The cold-air pool is substantially colder in the control run and it is associated with an excessive thermal gradient along the coast when compared to the reference run. In contrast, the cold-air pool temperatures in the coupled run are much closer to the values in the reference run. In addition, the thermal gradient for the coupled run, while not as strong as the reference run, is still a little more accurate than the gradient in the control run. In the figures, the 80% relative humidity contour is identified to give an indication of the amount of cloudiness each run is projecting. This is important regarding the radiation effects in the lower atmosphere. Typically in hydrostatic models such as NORAPS, which do not include an explicit cloud water variable, a stratiform cloud fraction is parameterized by an increasing quadratic function of the excess relative humidity above a certain threshold. The threshold value depends on pressure level (about 60% for low clouds, 50% for middle clouds, and 85% for high clouds). The cloud fraction then increases from zero at and below the threshold value to one at saturation. For the low levels shown in Fig. 20, the 80% relative humidity contour marks the boundary of 25% or greater cloud cover. While both the coupled and control runs overpredict the area covered by relative humidity values exceeding 80% compared to the reference run, the coupled is the better of the two. The control projects the 80% relative humidity line farther west into the cold air than does the coupled run. Having more cloud cover over the cold-air damming area could help explain why the temperatures close to the ground are cooler for the control run compared to the coupled and reference runs. It should be noted that the coupled forecast cross section matches quite closely with a subjectively analyzed cross section for nearly the same domain presented by Riordan (1990).

Another important aspect to examine when assimilating mass data without wind data is the effect of the mass fields on the wind fields. In ideal situations, the winds would properly adjust in response to updates of the mass fields, although there are dynamical constraints on the extent to which that can happen. In Figs. 21 and 22 the differences of wind speeds for the control and coupled runs from the reference run are presented for

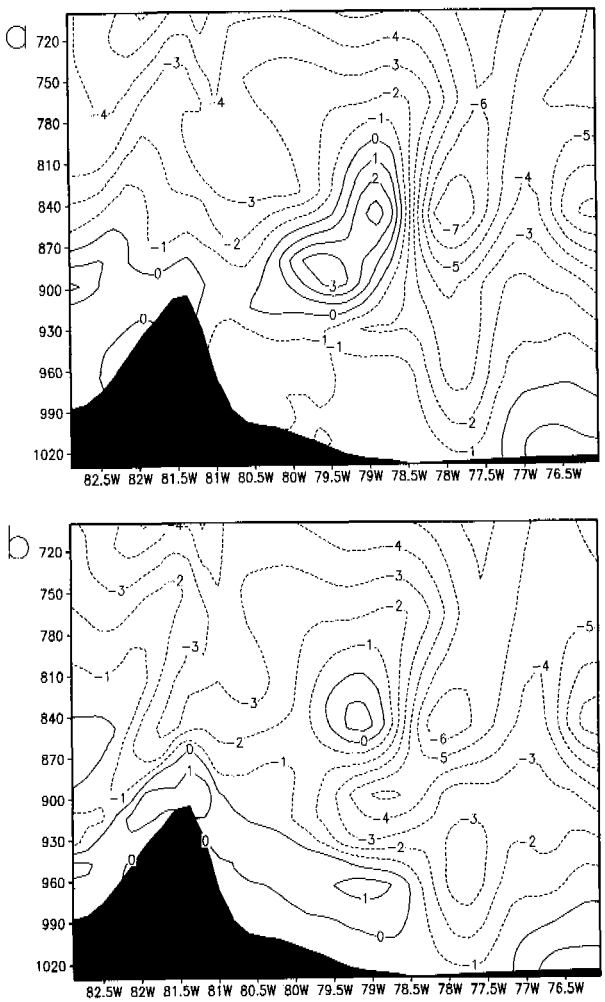

FIG. 21. Difference of wind speed component (contoured every m s^{-1}) normal to the cross section depicted in Fig. 20 relative to the reference run for (a) control run forecast and (b) coupled run forecast. Positive values are coming out of the page. Fields are valid at 0000 UTC 25 Jan 1986.

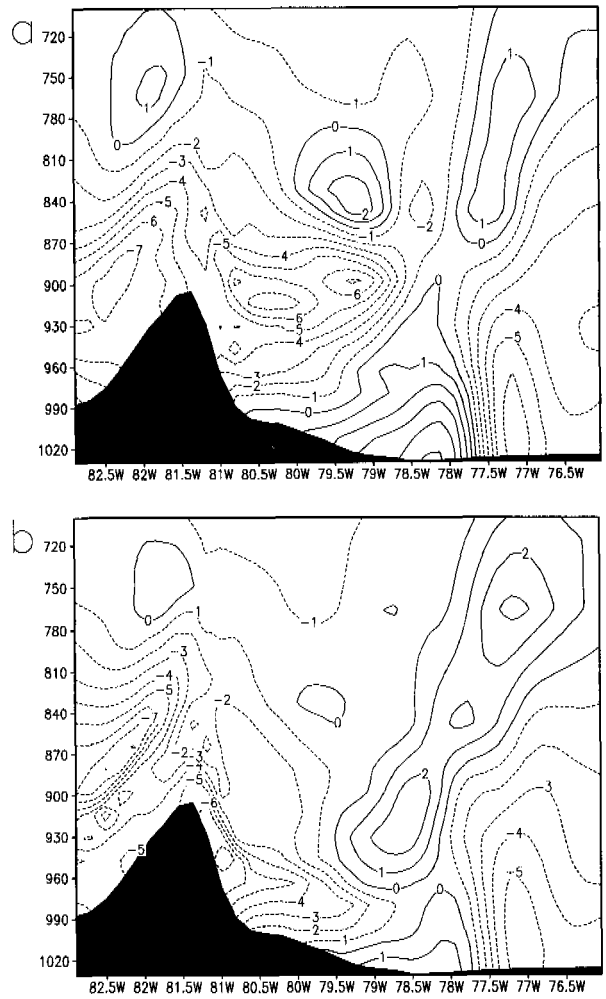

FIG. 22. Same as Fig. 21 except for wind speed tangential to the cross section with positive values to the right.

the cross section described above. Both the wind speed differences normal and tangential to the cross section are shown. Generally, the magnitude of the differences is less for the coupled run. In particular, for the normal wind, the coupled run is slightly more similar to the reference run in the area of the cold-air damming. The coupled and control runs bracket the reference run in this area, with the coupled run containing a more northeasterly flow within the cold air, which suggests that more realistic wind flow is captured by the coupled run. In the tangential wind field, both the coupled and control runs show increased convergence near the coast compared to the reference. However, the coupled run's deviation is less than the control run's. The control run's excessive deviation is most likely correlated with the fact that it has overdone the coastal thermal gradient.

Figure 23 shows the change in temperature for the cross section for each of the three runs between 0000 and 0600 UTC 25 January 1986. During this time the reference run exhibits strong nighttime cooling in the cold-air dome and also warming above it as the marine easterly flow is forced up and over the cold air. The coupled run depicts the strong warming that is occurring above the cold-air pool. In addition, the coupled run has far less warming occurring within the cold-air pool than does the control run. Thus in the coupled run, the warmer marine easterly flow is not eroding the cold air between the mountains and the developing coastal front as much as the control run. One reason for this difference is the geostrophic adjustment of the winds from the updating of the mass fields that occurs during the coupled run assimilation phase. It is the failure of the NORAPS surface physics parameterization to forecast the surface cooling that enables the marine air to erode the cold dome, to differing degrees, for the control and coupled forecasts. This has reduced the amount of the benefit that might have otherwise been seen in the NO-

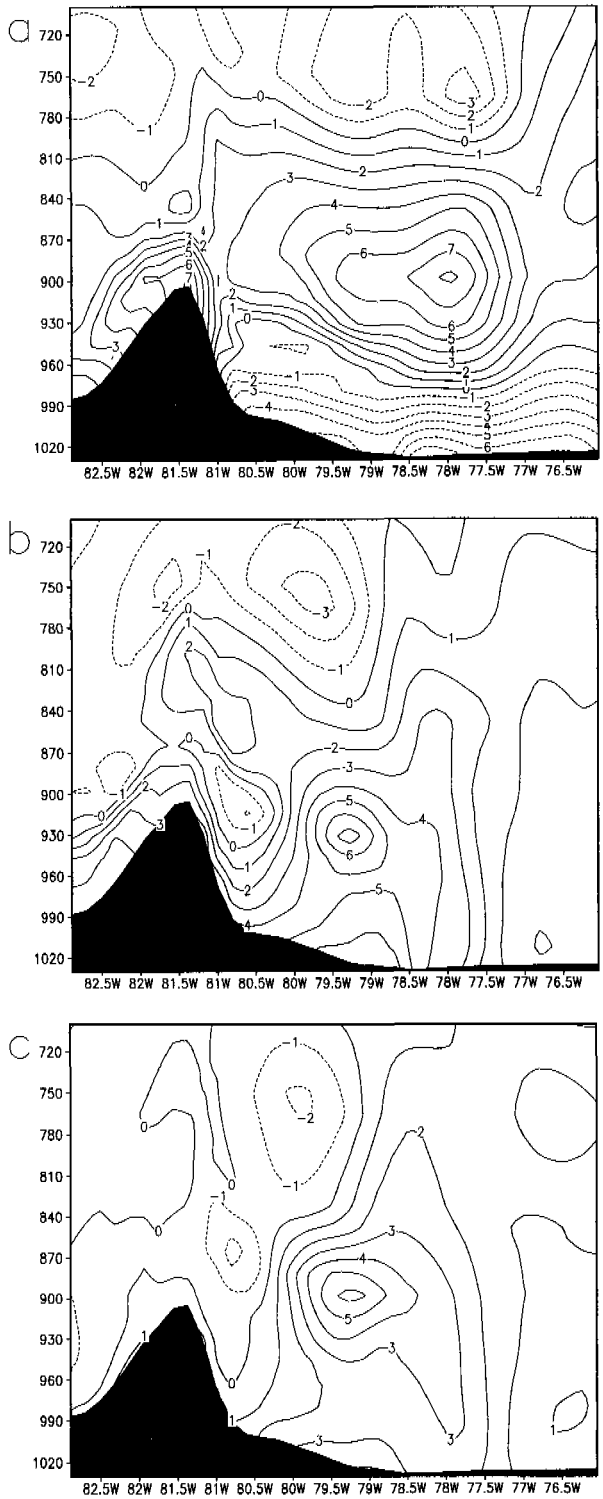

FIG. 23. Temperature change (contours every K) in cross section depicted in Fig. 21 from 0000 to 0600 UTC 25 Jan 1986 for (a) reference run, (b) control run forecast, and (c) coupled run forecast.

RAPS forecasts when assimilating VAS data for this case.

5. Summary and conclusions

The coupled procedure of assimilating geostationary satellite sounder data was adapted to a mesoscale forecast and analysis system being jointly developed by NRL and AFRL. In doing so, the Bratseth (1986) successive corrections objective analysis scheme was modified to account for the spatial correlation of the observation error. The entire procedure was applied to a cold-air damming, coastal frontogenesis case that occurred during the GALE project in 1986.

The retrievals generated from the coupled method were improved relative to independent stand-alone retrievals generated by NOAA/NESDIS. The coupled retrievals were not as accurate as the stand-alone retrievals above the tropopause due to poor first guesses produced by the model, which the retrieval process could not correct. When analyzed using the modified Bratseth approach, the stand-alone retrievals resulted in analyses very close in quality to analyses generated by the coupled retrievals. This indicates that there is substantial room for improvement in quantifying the errors used in the analysis, such as correlating the background errors with the observations and varying the background error with height. Comparisons of analyses from the coupled run with forecasts from the control run show the coupled analyses generally had better temperature and moisture fields. The amount of improvement was modest. However with better information on the retrieval error statistics and the use of the improved sounder on board GOES (Menzel and Purdom 1994), it should be possible to lower the assigned observation errors and thus make the analysis more responsive to the retrievals. In comparing the forecasts from both the coupled and control runs, the coupled run produced superior moisture forecasts. The coupled temperature forecasts were generally better than those from the control run in the short term (3 h). By the 9-h point of integration, the low-level temperatures in the coupled run were less accurate than on the control run; however, the coupled run appears to be better in depicting the mesoscale processes that sustained the cold-air pool.

Overall the results indicate the coupled approach yielded a positive impact of VAS data on the GALE case studied. Some aspects of the results were negatively affected by deficiencies in the NORAPS model's handling of the lower boundary condition. In cases of strong surface forcing in winter, such as our case of cold-air damming, large vertical temperature gradients can be produced at low levels near the surface by the nighttime radiational cooling followed by the daytime solar heating at the surface. The vertical averaging inherent in the retrieval methods requires that a good estimate of this vertical temperature gradient be provided by the first guess. In our case, the errors in the lower-level tem-

perature forecasts, due to problems in the NORAPS surface parameterization, can help explain the overwarming of the surface temperature seen in the coupled analysis at 1800 UTC 24 January 1986 and the subsequent erosion of the cold dome in the NORAPS forecast by the onshore marine air after 6–9 h of integration. The retrievals also could not correct errors in the temperature lapse rate forecast by NORAPS in the stratosphere, which had little impact on the lower-tropospheric features being studied in this case. To gain more from the assimilation of any IR sounder data in cases of strong mesoscale surface forcing, a more sophisticated land surface parameterization would be needed in the mesoscale model combined with a detailed description of the surface soil and vegetation characteristics. Furthermore, before operational implementation, the presented approach should be evaluated using a longer series of case studies involving many different synoptic situations and compared against other methods of assimilation.

Acknowledgments. The authors thank Gary Wade of NOAA/NESDIS in Madison, Wisconsin, and Randall Alliss and Kevin Schrab, both formerly of North Carolina State University, for their help in providing the VAS data for GALE IOP 2. The authors also thank Donald Chisholm, George Modica, and Donald Norquist of Air Force Research Laboratory, and an anonymous reviewer for their critiques of this manuscript. This work was supported in part by a grant of HPC time from the DoD centers at Vicksburg, Mississippi, and Wright-Patterson AFB, Ohio, for time on their CRAY C-90s and at NRL for time on the Cray Y-MP-EL.

APPENDIX

Approximation of the Correlated Observation Error

Using f to represent the deviation of a variable from a background field, each analysis point is updated by the Bratseth equation:

$$f_x^{m+1} = f_x^m + \sum_{j=1}^{n} \alpha_{xj}(f_j^o - f_j^m), \tag{A1}$$

where f_x is the updated value of f at grid point x, m is the iteration number, f_j^o is an observed value of f, f_j^m is the analysis estimate at the observation location from iteration m, and n is the number of observations that can affect the particular analysis point. The analysis estimate at the observation location is determined by

$$f_i^{m+1} = f_i^m + \sum_{j=1}^{n} \alpha_{ij}(f_j^o - f_j^m). \tag{A2}$$

Allowing the overbar notation to represent ensemble averages over a large number of cases then the weights, α, in (A1) and (A2) are

$$\alpha_{xj} = \frac{\overline{f_x^t f_j^o}}{M_j} \tag{A3}$$

and

$$\alpha_{ij} = \frac{\overline{f_i^o f_j^o}}{M_j}, \tag{A4}$$

where f_x^t is the deviation of the true value from the background field and M_j is the data density function and is given by

$$M_j = \sum_{k=1}^{n} \overline{f_j^o f_k^o}. \tag{A5}$$

The value of f^t is related to the observation by

$$f^o = f^t + \chi + \varepsilon, \tag{A6}$$

where χ is the spatially correlated part of the observation error and ε is the random part of the observation error. If we assume that the observation error is not spatially correlated with the synoptic features (which is not strictly valid in this case), then the covariance [the numerator in (A3)] can be modeled as in Sashegyi et al. (1993):

$$\overline{f_x^t f_j^o} = f_x^t f_j^t = \sigma_f^2 \rho_{xj}, \tag{A7}$$

where σ_f^2 is the variance of the background error and ρ_{xj} is the correlation function describing the spatial correlation of the background error between the grid point x and the observation location j. The background error correlation function is modeled as a Gaussian,

$$\rho_{xj} = e^{-r_{xj}^2/d^2}. \tag{A8}$$

The variable d is the length scale for the Gaussian distribution and r_{xj} is the distance between x and j. Using Eq. (A6), the numerator of (A4) becomes

$$\overline{f_i^o f_j^o} = \overline{(f_i^t + \chi_i + \varepsilon_i)(f_j^t + \chi_j + \varepsilon_j)}. \tag{A9}$$

Noting that ε is random and assuming that χ is not correlated with f^t, then the expansion of (A9) can be reduced to the following:

$$\overline{f_i^o f_j^o} = \overline{f_i^t f_j^t} + \overline{\chi_i \chi_j} + \overline{\varepsilon_i \varepsilon_j}, \tag{A10}$$

which can be rewritten as

$$\overline{f_i^o f_j^o} = \sigma_f^2 \rho_{ij} + \sigma_\chi^2 \mu_{ij} + \sigma_\varepsilon^2 \delta_{ij}, \tag{A11}$$

where σ_χ^2 is the variance of the spatially correlated observation error, σ_ε^2 is the variance of the random observation error, and δ_{ij} is the Kronecker delta function where $\delta = 1$ for $i = j$ and $\delta = 0$ otherwise. The function μ gives the spatial correlation for the observation error and has the same Gaussian form (with a different length scale) as the background error correlation function in (A8). Likewise, the data density function in (A5) can be modified to also include spatially correlated error:

$$M_j = \sum_{k=1}^{n} \sigma_f^2 \rho_{ik} + \sigma_\chi^2 \mu_{ik} + \sigma_\varepsilon^2 \delta_{ik}. \tag{A12}$$

REFERENCES

Andersson, E., J. Pailleux, J.-N. Thépaut, J. R. Eyre, A. P. McNally, G. A. Kelly, and P. Courtier, 1994: Use of cloud-cleared radiances in three/four dimensional variational data assimilation. *Quart. J. Roy. Meteor. Soc.*, **120,** 627–653.

Arakawa, A., and V. R. Lamb, 1977: Computational design of the basic dynamical processes of the UCLA general circulation model. *Methods in Computational Physics,* J. Chang, Ed., *General Circulation Models of the Atmosphere,* Academic Press, 173–265.

Barnes, S. L., 1964: A technique for maximizing details in numerical weather map analysis. *J. Appl. Meteor.*, **3,** 396–409.

——, 1994a: Applications of the Barnes objective analysis scheme. Part I: Effects of undersampling, wave position, and station randomness. *J. Atmos. Oceanic Technol.*, **11,** 1433–1448.

——, 1994b: Applications of the Barnes objective analysis scheme. Part II: Improving derivative estimates. *J. Atmos. Oceanic Technol.*, **11,** 1449–1458.

——, 1994c: Applications of the Barnes objective analysis scheme. Part III: Tuning for minimum error. *J. Atmos. Oceanic Technol.*, **11,** 1459–1479.

Bell, G. D., and L. F. Bosart, 1988: Appalachian cold-air damming. *Mon. Wea. Rev.*, **116,** 137–161.

Blackadar, A. K., 1979: High resolution models of the planetary boundary layer. *Advances in Environmental Science and Engineering,* J. R. Pfafflin and E. N. Ziegler, Eds., Vol. 1, Gordon and Breach, 50–85.

Bratseth, A. M., 1986: Statistical interpolation by means of successive corrections. *Tellus,* **38A,** 439–447.

Carr, F. H., J. M. Krause, and K. Brewster, 1996: Application of the Bratseth scheme to high-resolution analyses in inhomogenous data regimes. Preprints, *15th Conf. on Weather Analysis and Forecasting,* Norfolk, VA, Amer. Meteor. Soc., 231–234.

Daley, R., 1991: *Atmospheric Data Analysis.* Cambridge University Press, 457 pp.

Davies, H. C., 1976: A lateral boundary formulation for multi-level prediction models. *Quart. J. Roy. Meteor. Soc.*, **102,** 405–418.

Detering, H. W., and D. Etling, 1985: Application of the E-ε turbulence model to the atmospheric boundary layer. *Bound.-Layer Meteor.*, **33,** 113–133.

Doyle, J. D., and T. T. Warner, 1990: Mesoscale coastal processes during GALE IOP 2. *Mon. Wea. Rev.*, **118,** 283–308.

Fleming, H. E., and L. M. McMillin, 1977: Atmospheric transmittance of an absorbing gas. 2: A computationally fast and accurate transmittance model for slant paths at different zenith angles. *Appl. Opt.*, **16,** 1366–1370.

Gadd, A. J., B. R. Barwell, S. J. Cox, and R. J. Renshow, 1995: Global processing of satellite sounding radiances in a numerical weather prediction system. *Quart. J. Roy. Meteor. Soc.*, **121,** 615–630.

Harshvardhan, R. Davies, D. A. Randall, and T. G. Corsetti, 1987: A fast radiation parameterization for atmospheric circulation models. *J. Geophys. Res.*, **92,** 1009–1016.

Hayden, C. M., 1988: GOES-VAS simultaneous temperature-moisture retrieval algorithm. *J. Appl. Meteor.*, **27,** 705–733.

——, G. S. Wade, and T. J. Schmit, 1996: Derived product imagery from GOES-8. *J. Appl. Meteor.*, **35,** 153–162.

Hodur, R. M., 1987: Evaluation of a regional model with an update cycle. *Mon. Wea. Rev.*, **115,** 2707–2718.

Keeter, K. K., S. Businger, L. G. Lee, and J. S. Waldstreicher, 1995: Winter weather forecasting throughout the eastern United States. Part III: The effects of topography and the variability of winter weather in the Carolinas and Virginia. *Wea. Forecasting,* **10,** 42–60.

Kuo, H.-L., 1974: Further studies of the parameterization of the influence of cumulus convection on large scale flow. *J. Atmos. Sci.*, **31,** 1232–1240.

Liou, C.-S., C. H. Wash, S. M. Heikkinen, and R. L. Elsberry, 1990: Numerical studies of cyclogenesis events during the Second Intensive Observation Period (IOP-2) of GALE. *Mon. Wea. Rev.*, **118,** 218–233.

——, R. M. Hodur, and R. H. Langland, 1994: Navy Operational Atmospheric Prediction System (NORAPS): A triple nested mesoscale model. Preprints, *10th Conf. on Numerical Weather Prediction,* Portland, OR, Amer. Meteor. Soc., 423–425.

Lipton, A. E., 1993: Cloud shading retrieval and assimilation in a satellite-model coupled mesoscale analysis system. *Mon. Wea. Rev.*, **121,** 3062–3081.

——, and T. H. Vonder Haar, 1990a: Mesoscale analysis by numerical modeling coupled with sounding retrievals from satellites. *Mon. Wea. Rev.*, **118,** 1308–1329.

——, and ——, 1990b: Preconvective mesoscale analysis over irregular terrain with a satellite-model coupled system. *Mon. Wea. Rev.*, **118,** 1330–1358.

——, G. D. Modica, S. T. Heckman, and A. J. Jackson, 1995: Satellite-model coupled analysis of convective potential in Florida with VAS water vapor and surface temperature data. *Mon. Wea. Rev.*, **123,** 3292–3304.

Louis, J.-F., 1979: A parametric model of vertical eddy fluxes in the atmosphere. *Bound.-Layer Meteor.*, **17,** 187–202.

Madala, R. V., 1981: Efficient time integration schemes for atmosphere and ocean models. *Finite Difference Techniques for Vectorized Fluid Dynamic Calculations,* D. L. Book, Ed., Springer-Verlag, 56–74.

——, S. W. Chang, U. C. Mohanty, S. C. Madan, R. K. Paliwal, V. B. Sarin, T. Holt, and S. Raman, 1987: Description of the Naval Research Laboratory limited area dynamical weather prediction model. NRL Memo. Rep. 5992, Naval Research Laboratory, Washington, DC, 132 pp. [NTIS A182780.]

Manabe, S., J. Smagorinsky, and R. F. Strickler, 1965: Simulated climatology of a general circulation model with a hydrologic cycle. *Mon. Wea. Rev.*, **93,** 769–798.

McMillin, L. M., and H. E. Fleming, 1976: Atmospheric transmittance of an absorbing gas: A computationally fast and accurate transmittance model for absorbing gases with constant mixing ratios in homogeneous atmospheres. *Appl. Opt.*, **15,** 358–363.

Menzel, W. P., and J. F. W. Purdom, 1994: Introducing GOES-I: The first of a new generation of Geostationary Operational Environmental Satellites. *Bull. Amer. Meteor. Soc.*, **75,** 757–781.

——, W. L. Smith, G. S. Wade, L. D. Herman, and C. M. Hayden, 1983: Atmospheric soundings from a geostationary satellite. *Appl. Opt.*, **22,** 2686–2689.

Monin, A. S., and A. M. Obukhov, 1954: Basic laws of turbulent mixing in the atmosphere near the ground. *Tr. Akad. Nauk. SSSR Geophiz. Inst.*, **24,** 1963–1987.

Parrish, D. F., and J. C. Derber, 1992: The National Meteorological Center's spectral statistical-interpolation analysis system. *Mon. Wea. Rev.*, **120,** 1747–1763.

Perkey, D. J., and C. W. Kreitzberg, 1976: A time-dependent lateral boundary scheme for limited-area primitive equation models: *Mon. Wea. Rev.*, **104,** 744–755.

Riordan, A. J., 1990: Examination of the mesoscale features of the GALE coastal front of 24–25 January 1986. *Mon. Wea. Rev.*, **118,** 258–282.

Robert, A. J., 1966: The integration of a low order spectral form of the primitive meteorological equations. *J. Meteor. Soc. Japan,* **44,** 237–245.

Ruggiero, F. H., K. D. Sashegyi, R. V. Madala, and S. Raman, 1996: The use of surface observations in four-dimensional data assimilation with a mesoscale model. *Mon. Wea. Rev.*, **124,** 1018–1033.

Sashegyi, K. D., and R. V. Madala, 1993: Application of vertical-mode initialization to a limited-area model in flux form. *Mon. Wea. Rev.*, **121,** 207–220.

——, D. F. Harms, R. V. Madala, and S. Raman, 1993: Application of the Bratseth scheme for the analysis of GALE data using a mesoscale model. *Mon. Wea. Rev.*, **121,** 2331–2350.

——, R. V. Madala, D. E. Harms, and S. Raman, 1994: A numerical weather prediction system for regional and mesoscale forecasting

on a high performance workstation. Preprints, *10th Conf. on Numerical Weather Prediction*, Portland, OR, Amer. Meteor. Soc., 363–365.

Schlatter, T. W., and G. W. Branstator, 1979: Estimation of errors in Nimbus 6 temperature profiles and their spatial correlation. *Mon. Wea. Rev.*, **107,** 1402–1413.

Smith, W. L., H. M. Woolf, P. G. Abel, C. M. Hayden, M. Chalfant, and N. Grody, 1974: Nimbus-5 Sounder Data Processing System. Part I: Measurement characteristics and data reduction procedures. NOAA Tech. Memo. NESS 57, 99 pp. [NTIS COM74114361AS.]

Stauffer, D. R., and N. L. Seaman, 1990: Use of four-dimensional data assimilation in a limited-area mesoscale model. Part I: Experiments with synoptic-scale data. *Mon. Wea. Rev.*, **118,** 1250–1277.

Thompson, O. E., and M. T. Tripputi, 1994: NWP-initialized satellite temperature retrievals using statistical regularization and singular value decomposition methods. *Mon. Wea. Rev.*, **122,** 897–926.

Tiedtke, M., W. A. Heckley, and J. Slingo, 1988: Tropical forecasting at ECMWF: The influence of physical parameterization on the mean structure of forecasts and analysis. *Quart. J. Roy. Meteor. Soc.*, **114,** 639–664.

Weinreb, M. P., and A. C. Neuendorffer, 1973: Method to apply homogeneous-path transmittance models to inhomogeneous atmospheres. *J. Atmos. Sci.*, **30,** 662–666.